Robotics and Autonomous Systems 115 (2019) 83–89

Contents lists available at ScienceDirect

Robotics and Autonomous Systems

journal homepage: www.elsevier.com/locate/robot

Implementation and testing of a sideslip estimation for a formula student prototype

André Antunes [b], Pedro Outeiro [a,b,*], Carlos Cardeira [a,b], Paulo Oliveira [a,b]

[a] IDMEC, Universidade de Lisboa, Avenida Rovisco Pais, 1049-001 Lisboa, Portugal
[b] Instituto Superior Técnico, Universidade de Lisboa, Avenida Rovisco Pais, 1049-001 Lisboa, Portugal

HIGHLIGHTS

- Sideslip estimation was achieved using low-cost sensors.
- Testing was performed with data acquired from a Formula Student race car.
- Testing was performed in real time at 100 Hz using a RC car.
- The Burckhardt Tire Model was used providing easier implementation on other vehicles.

ARTICLE INFO

Article history:
Available online 13 February 2019

Keywords:
Kalman Filters
Estimation
System implementation
Real-time systems
Vehicle dynamics

ABSTRACT

This document details the implementation and test of a self-calibrating estimation architecture for the sideslip of a Formula Student prototype. The proposed algorithm fuses several sensors being the most relevant an Inertial Measurement Unit (IMU) and a Global Positioning System (GPS). It is presented a comparison between a linear and a non-linear estimators, and their consequences. The algorithm is tested with real data from a Formula Student vehicle, and validated with a differential GPS. It is also reported an implementation of the proposed algorithm in a micro-controller, and tested with a radio-controlled (RC) vehicle. These results are also validated with the data from a more accurate indoor motion system.

1. Introduction

For several years, the Formula Student has been challenging university students from all around the world to develop and construct single-seat formula style racing vehicles. From interaction between students and teams with the objective of building a better and more advanced vehicle, and driven by the organization, the competition has been evolving from year to year. Starting with a simple steel chassis with a motorcycle combustion engine to the more recent composite chassis and aerodynamic devices, with self-developed electric motors with four-wheel drive, the Formula Student has always strived to be side-by-side with the automotive industry. On the summer of 2017, a new competition took place, the Formula Student Driverless (FSD). This one is in all identical to the previous, with the exception that the vehicles are completely autonomous in the track. By participating in the Formula Student team, it was possible to learn about the inner workings of cars, electronics, aerodynamics, how to manage and work in large projects. It also provides an opportunity to gain contacts with companies, as a major part of the project is finding sponsors willing to provide components for the prototype.

Since the adoption of electric motors, new control strategies started to be implemented, being the more common ones the traction control and torque-vectoring or electronic differential.

The implementation of these features in an automobile requires new sensors and actuators to be installed, like wheel encoders and IMUs. With the presence of a driver the implementation was easier, since he is able to make small corrections to keep the car in a stable condition. In this new driverless competition, the control problem had to be rethought, and a new need arose for more sensors and/or more information to compensate for the lack of a driver.

Due to the power weight ratio of the Formula Student vehicles, they have a clear tendency to become unstable (loss of grip), especially in curves. This implies that it is necessary to have information of the sideslip of the vehicle specially when using controllers that work close to the stability limit of the vehicle as exposed in the works [1–3]. In [1] the use of two second-order sliding-mode controllers is compared against a feedforward controller combined with either a conventional or an adaptive PID controller. In [2] a control scheme based on a fuzzy rule-based body slip angle (beta) observer is studied, while [3] proposes a differential braking

* Corresponding author at: Instituto Superior Técnico, Universidade de Lisboa, Avenida Rovisco Pais, 1049-001 Lisboa, Portugal.
E-mail addresses: andre.antunes@tecnico.ulisboa.pt (A. Antunes), pedro.outeiro@tecnico.ulisboa.pt (P. Outeiro), carlos.cardeira@tecnico.ulisboa.pt (C. Cardeira), paulo.j.oliveira@tecnico.ulisboa.pt (P. Oliveira).

https://doi.org/10.1016/j.robot.2019.01.018
0921-8890/

control law based on vehicle planar motion using a three-degree-of-freedom yaw plane vehicle model.

The most direct method of observing the sideslip angle is to use a dedicated sensor, such as a Differential Global Positioning System (DGPS) or an optical sensor or optical flow like the Correvit® family sensor as used in [4], where a dynamic modeling and observation method to estimate tire-road forces and sideslip angle is presented. These sensors have some issues associated with their usage. Both systems are heavy and bulky in relation to a Formula Student vehicle. The DGPS besides the clear line of sight to the sky, also needs some warm up time to have some feasible data. The optical flow sensors need regular calibrations to maintain their accuracy.

Due to the issues associated with the dedicated sensors, several research groups try to create a sideslip observer using different techniques. Most of these works use sensors like an IMU and/or GPS like [5,6], and the dynamic equations of the vehicle. A method that utilizes a two-antenna GPS system to provide direct measurements of vehicle roll and heading, resulting in improved sideslip estimation is proposed in [5], while [6] designed a sideslip observer that has less tuning parameters and is less computationally demanding than an Extended Kalman Filter. Works regarding sideslip observers commonly use the Kalman Filter [5] or the Extended Kalman Filter, but some other works like [4] explore the use of the Unscented Kalman Filter, or even neural networks as in [7], where the neural network is used to identify the patterns in the accelerations that correspond to sideslip excursions during drifts. This work presents the implementation of a self-calibrating estimation architecture already presented for simulation in [8] and the first results in [9]. The proposed architecture is composed of an Attitude Complementary Filter, a Position Complementary Filter, and a Vehicle Model Estimator. Additionally, the attitude estimation relies on cheap sensors, namely a magnetometer and a gyroscope, and provided satisfactory results. In these two papers, only linear approaches were considered for the Attitude Complementary Filter. The proposed algorithm uses the fusion of an IMU with a GPS, that uses kinematic equations. The estimators proposed are both Kalman Filter and Extended Kalman Filter solutions [10]. This document deals with the testing of the non-linear estimator in comparison with the linear one, and the implementation of the algorithm in a micro-controller.

In Section 2 the estimator architecture introduced by [8,9], with the equations and assumptions used, is detailed, in Section 3 the testing and validation of the algorithm is performed using real data from a Formula Student prototype. Section 4 illustrates the implementation of the algorithm in a micro-controller and the results obtained during real test drive conditions are discussed. Finally, in Section 5, a small overview of all the results obtained is presented.

2. Estimator architecture

To obtain the sideslip estimate, the architecture presented in Fig. 1 is used. This architecture is composed by three main filters. The first is an Attitude Complementary Filter (ACF), that uses the yaw readings from the magnetometer and the yaw rate reading from a gyroscope to provide a filtered yaw angle of the vehicle and an estimate of the yaw rate bias to correct the signal from the sensor. The second one is a Position Complementary Filter (PCF), which merges the position and accelerations to provide an estimate of the velocity components. This filter is also self-calibrated since it also accounts for the bias in the accelerometer. The last filter is the Vehicle Estimator (VE). For this one, two types of estimators are compared, one linear and one non-linear. These filters are based on first physics principles that are used to model the planar motion equations of a vehicle, that rely on the velocity components, yaw

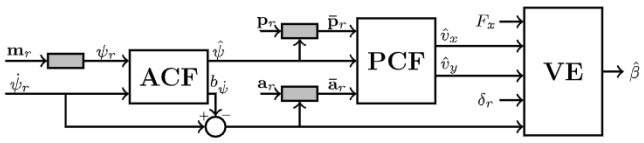

Fig. 1. Architecture of the estimator where $\mathbf{m}_r$, $\dot{\psi}_r$, $\mathbf{a}_r$, $\mathbf{p}_r$, δ_r and F_x are respectively the measurements from the magnetometer, gyroscope, accelerometer, GPS, steering encoder and force by the motors. Gray boxes represent data processing blocks to be detailed.

rate and steering angle to provide the sideslip estimate. The non-linear filter also uses the longitudinal force applied on the vehicle.

Alongside these three main filters, three signal pre-processors are used to prepare the measurements. The first is a conversion of the magnetic components of a magnetometer to the yaw angle, assuming that the magnetic components are properly calibrated. The second is to transpose the position of the receptor to the center of gravity (CG). The third is the transformation of the acceleration reading to a $\partial v/\partial t$ signal used by the PCF.

In this section, the three main filters are detailed and their equations deduced. First the kinematic filters, and after the vehicle estimators.

2.1. Attitude complementary filter

The ACF fuses the yaw angle measurements (ψ_r) with the angular velocity around the z-axis, or yaw rate ($\dot{\psi}_r$), to deliver a more accurate yaw angle ($\hat{\psi}$) value. It is considered that the yaw from the magnetometer is already calibrated as proposed in [11]. The ACF also provides a bias ($b_{\dot{\psi}}$) estimate for the yaw rate reading, in order to account for the static and dynamic offsets of the gyroscope. This bias is later used to correct the yaw rate for the following filters.

This filter is based on the discrete kinematic equation for the yaw angle given by (1), where k defines the time instant $t = kT$ being T the sampling time.

$$\psi_{k+1} = \psi_k + T\dot{\psi}_k \tag{1}$$

It is assumed that the yaw measurement ((2)a) is corrupted by Gaussian white-noise ($w_{\psi_r,k}$) as well as the yaw rate reading ($w_{\dot{\psi}_r,k}$), and the evolution of the bias ((2)b) is also driven by Gaussian white noise ($w_{b_{\dot{\psi}},k}$).

$$\psi_{r,k} = \psi_k + w_{\psi_r,k} \tag{2a}$$

$$\dot{\psi}_{r,k} = \dot{\psi}_k + b_{\dot{\psi},k} + w_{\dot{\psi}_r,k}\,, \quad b_{\dot{\psi},k+1} = b_{\dot{\psi},k} + w_{b_{\dot{\psi}},k} \tag{2b}$$

With the combination of Eqs. (1) and (2), it is possible to write the discrete attitude complementary filter (3), where K_1 and K_2 are the time-invariant Kalman gains identified, and v_k the noise associated with the yaw angle reading.

$$\begin{bmatrix}\psi_{k+1}\\ b_{\dot{\psi},k+1}\end{bmatrix} = \begin{bmatrix}1 & -T\\ 0 & 1\end{bmatrix}\begin{bmatrix}\psi_k\\ b_{\dot{\psi},k}\end{bmatrix} + \begin{bmatrix}T\\ 0\end{bmatrix}\dot{\psi}_r + \begin{bmatrix}K_1\\ K_2\end{bmatrix}(y_k - \hat{y}_k)$$
$$y_k = \psi_{r,k} + v_k \quad , \quad \hat{y}_k = \hat{\psi}_k \tag{3}$$

2.2. Position complementary filter

The PCF is used to estimate the velocity components in the body referential. It uses the position provided by the GPS and the planar accelerations from the on-board accelerometer. The yaw angle from the ACF is applied to convert the components to the body referential. This filter is also kinematic, as the previous, using the equations of motion as described by (4), where $\mathcal{R}_k$ represents the rotation matrix that makes the conversion from the body frame

to the global frame, using the yaw estimate from the ACF at the instant k.

$$\bar{\mathbf{p}}^G_{k+1} = \bar{\mathbf{p}}^G_k + T\bar{\mathbf{v}}^G_k + \frac{T^2}{2}\mathcal{R}_k\bar{\mathbf{a}}^B_{rk} \tag{4a}$$

$$\bar{\mathbf{v}}^G_{k+1} = \bar{\mathbf{v}}^G_k + T\mathcal{R}_k\bar{\mathbf{a}}^B_{rk} \tag{4b}$$

It is assumed that both measurements, position and acceleration, are corrupted with Gaussian random white-noise, $\bar{\mathbf{w}}_{pk}$ and $\bar{\mathbf{w}}_{ak}$ respectively. Besides that, it is also assumed that the acceleration readings also have bias, due to the sensor offset and the influence of roll and pitch as described by (5), which is also driven by Gaussian white-noise $\bar{\mathbf{w}}_{b_ak}$.

$$\bar{\mathbf{a}}^B_{rk} = \bar{\mathbf{a}}^B_k + \bar{\mathbf{b}}^B_{ak} + \bar{\mathbf{w}}_{ak} \tag{5a}$$

$$\bar{\mathbf{b}}_{ak+1} = \bar{\mathbf{b}}_{ak} + \bar{\mathbf{w}}_{b_ak} \tag{5b}$$

Using Eqs. (4) and (5), then it is possible to write the PCF state space system as (6), where I is a 2×2 identity matrix.

$$\begin{bmatrix} \bar{\mathbf{p}}^G_{k+1} \\ \bar{\mathbf{v}}^B_{k+1} \\ \bar{\mathbf{b}}^B_{a(k+1)} \end{bmatrix} = \begin{bmatrix} I & T\mathcal{R}_k & -\frac{T^2}{2}\mathcal{R}_k \\ 0 & I & -TI \\ 0 & 0 & I \end{bmatrix} \begin{bmatrix} \bar{\mathbf{p}}^G_k \\ \bar{\mathbf{v}}^B_k \\ \bar{\mathbf{b}}^B_{ak} \end{bmatrix} + \begin{bmatrix} \frac{T^2}{2}\mathcal{R}_k \\ TI \\ 0 \end{bmatrix} \bar{\mathbf{a}}^B_{rk} + \begin{bmatrix} K_1 \\ \mathcal{R}^T_k K_2 \\ \mathcal{R}^T_k K_3 \end{bmatrix} \bar{e}_k \tag{6}$$

$$\bar{e}_k = (y_{\bar{p}k} - \hat{y}_{\bar{p}k}) \quad , \quad \hat{y}_{\bar{p}k} = \hat{\mathbf{p}}^G_k \quad , \quad y_{\bar{p}k} = \bar{\mathbf{p}}^G_{rk} + \bar{\mathbf{w}}_{pk}$$

The gains K_1, K_2 and K_3 are 2×2 diagonal matrices with the Kalman gains identified using the discrete Kalman Filter with the time-invariant equivalent of (6) where the estimated yaw is zero ($\hat{\psi}_k = 0$).

2.3. Vehicle estimator

The vehicle estimator is based on the planar movement equations [12] which implies that no roll or pitch are considered. It is assumed that the only forces applied on the vehicle are on the tires as presented in Fig. 2(a).

Each tire is presumed to generate a longitudinal (F_x) and a lateral (F_y) force in the wheel frame $\{w\}$. It is also assumed that left and right tires generate the same forces and can be combined as (7).

$$\begin{aligned} F^F_x &= F^{FL}_x + F^{FR}_x \quad , \quad F^R_x = F^{RL}_x + F^{RR}_x \\ F^F_y &= F^{FL}_y + F^{FR}_y \quad , \quad F^R_y = F^{RL}_y + F^{RR}_y \end{aligned} \tag{7}$$

Eqs. (8) result from the balance of forces to the vehicle, Fig. 2(a).

$$\dot{v}_x = v_y\dot{\psi} - \frac{1}{m}[F^F_y \sin\delta - F^F_x \cos\delta - F^R_x] \tag{8a}$$

$$\dot{v}_y = -v_x\dot{\psi} + \frac{1}{m}[F^F_y \cos\delta + F^R_y + F^F_x \sin\delta] \tag{8b}$$

$$\ddot{\psi} = \frac{1}{I_\psi}a[F^F_y \cos\delta + F^F_x \sin\delta] - \frac{1}{I_\psi}bF^R_y \tag{8c}$$

For simplification purposes is assumed that the longitudinal force is applied directly at the CG, and no longitudinal force is generated by the front wheels. The lateral force is dependent of the slip angle (α_i) of the tire, Fig. 2(b). This slip angle is defined as the difference between the sideslip angle of the vehicle projected in the wheel (β_i), and the steering angle of the wheel (δ), as given by (9). The projection of the sideslip angle on the wheel is then given by β_i, where x_i and y_i are the coordinates from the CG to the wheel i.

$$\alpha_i = \beta_i - \delta_i \ , \quad \beta_i = \mathrm{tg}^{-1}\left(\frac{v_y + x_i\dot{\psi}}{v_x - y_i\dot{\psi}}\right) \tag{9}$$

2.3.1. Vehicle linear estimator

The Vehicle Linear Estimator (VLE), uses a linearization of (8) with the assumption of small angles and a constant longitudinal velocity ($v_x \approx const$). This is a widely used approximation as seen in [13,14]. The lateral force generated by the tires is given by a cornering stiffness approximation (10). This one is a linearization to a typical tire model curve, also for small angles. The main issue with this approximation is the lack of lateral force saturation. This means that if the slip angle increases beyond the limits of the approximation, the force will acquire unrealistic values.

$$F_y = -C_\alpha\alpha \tag{10}$$

Combining Eqs. (8) to (10), and applying the assumptions described above it is possible to write the time-variant system (11) which is the starting point for the VLE.

$$\begin{bmatrix} \dot{v}_y \\ \ddot{\psi} \end{bmatrix} = \begin{bmatrix} -\frac{C_{\alpha f} + C_{\alpha r}}{m v_x} & -\frac{aC_{\alpha f} + bC_{\alpha r}}{m v_x} - v_x \\ -\frac{aC_{\alpha f} - bC_{\alpha r}}{I_\psi} & \frac{-a^2C_{\alpha f} + b^2C_{\alpha r}}{I_\psi v_x} \end{bmatrix} \begin{bmatrix} v_y \\ \dot{\psi} \end{bmatrix} + \begin{bmatrix} \frac{C_{\alpha f}}{m} \\ \frac{aC_{\alpha f}}{I_\psi} \end{bmatrix} \delta \tag{11}$$

For this estimator, four inputs are required. The sideslip computed as $\beta = \mathrm{tg}^{-1}(v_y/v_x)$ from the PCF and the yaw rate with the bias correction from the ACF are used as observations of the system. The steering angle is used as a direct input, and the longitudinal velocity is the element that makes this system time-varying, also used as a direct input.

Since the main objective is to implement the estimators in an on-board device, is useful to use discrete systems. To achieve the discrete equivalent of (11), property (12) is used to make the continuous to discrete conversion, where T is the sampling time, I is the identity matrix, A_k and B_k are the resulting discrete transition and input matrices, respectively, at instant k.

$$\exp\left(\begin{bmatrix} A_c & B_c \\ 0 & 0 \end{bmatrix} T\right) = \begin{bmatrix} A_k & B_k \\ 0 & I \end{bmatrix} \tag{12}$$

The continuous matrices A_c and B_c come from system (11). The estimator can be written as (13), where K_1 to K_4 are the discrete Kalman gains identified using the discrete equivalent system.

$$\begin{aligned} \begin{bmatrix} \hat{v}_{yk+1} \\ \hat{\dot{\psi}}_{k+1} \end{bmatrix} &= A_k \begin{bmatrix} \hat{v}_{yk} \\ \hat{\dot{\psi}}_k \end{bmatrix} + B_k\delta_r + \begin{bmatrix} K_1 & K_2 \\ K_3 & K_4 \end{bmatrix} (y_k - \hat{y}_k) \\ y_k &= \begin{bmatrix} v_{yk} \\ \dot{\psi}_k \end{bmatrix} + \begin{bmatrix} w_{vyk} \\ w_{\psi k} \end{bmatrix} \quad , \quad \hat{y}_k = \begin{bmatrix} \hat{v}_{yk} \\ \hat{\dot{\psi}}_k \end{bmatrix} \end{aligned} \tag{13}$$

2.3.2. Vehicle Non-Linear Estimator

The Vehicle Non-Linear Estimator (VNLE) also uses system (8) as a starting point, but without the small angle approximations. Additionally, like the previous estimator, it is useful to have the system in a discrete form, and for that (8) is discretized using Euler method, where the accelerations are replaced by (14). Since the sampling time is small, and the filter works in a close-loop, the error induced by this approximation is negligible. The discrete equivalent is then given by (15).

$$\dot{v}_x = \frac{v_{x_{k+1}} - v_{x_k}}{T} \quad , \quad \dot{v}_y = \frac{v_{y_{k+1}} - v_{y_k}}{T} \quad , \quad \ddot{\psi}_y = \frac{\dot{\psi}_{k+1} - \dot{\psi}_k}{T} \tag{14}$$

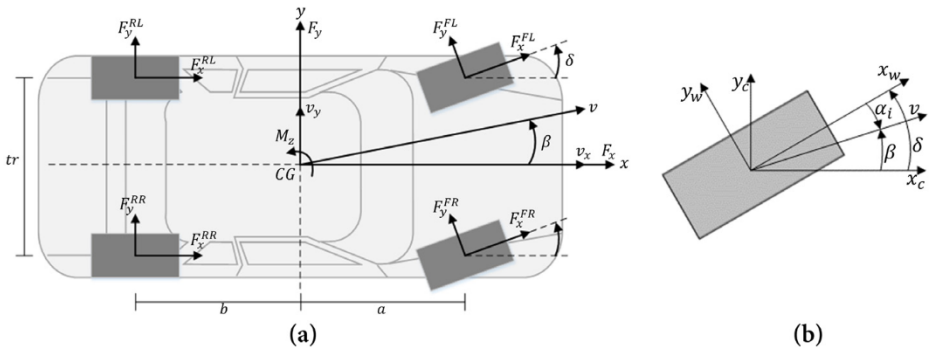

Fig. 2. (a) Forces applied on the Car; (b) Tire angles and frames, $\{w\}$ for wheel and $\{c\}$ for car.
Source: Image from [9].

$$v_{x_{k+1}} = v_{x_k} + v_{y_k}\dot{\psi}T - \frac{1}{m}\left[F_y^F \sin\delta - F_x\right]T \tag{15a}$$

$$v_{y_{k+1}} = v_{y_k} - v_{x_k}\dot{\psi}T + \frac{1}{m}\left[F_y^F \cos\delta + F_y^R\right]T \tag{15b}$$

$$\dot{\psi}_{k+1} = \dot{\psi}_k + \frac{1}{I_\psi}aF_y^F \cos\delta T - \frac{1}{I_\psi}bF_y^R T \tag{15c}$$

The lateral force for the VNLE is given by the Burckhardt tire model [15] which is expressed by (16), where c_1, c_2, c_3 and c_5 are the dry asphalt values proposed by the model. This equation already has two assumptions implemented. The first is the negligence of the velocity influence for simplification. And the second is the assumption of only driving and no braking. The Burckhardt model was chosen, as it provides a simpler behavior, although effective for the purposes at hand, than other alternatives, like the Magic Formula. Additionally, the parameters of the Burckhardt model can be obtained from a table of road conditions, without the need for performing model identification for the tires.

$$F_y = sign(\alpha)\left(c_1\left(1 - e^{-c_2 s_r}\right) - c_3 s_r\right)\left(1 - c_5 F_z^2\right)F_z\ , \quad s_r = |\tan\alpha| \tag{16}$$

The VNLE is created it resource to the Discrete Extended Kalman Filter [10]. It uses three observations, longitudinal velocity and lateral velocity from the PCF and the bias corrected yaw rate from the ACF. Also uses the steering angle as the input, and the longitudinal force as a direct influence in the system. The equations of the VNLE are not presented due to their extension.

3. Application on a formula student prototype

To test the algorithm, real data from a formula student car was retrieved. At the time available for the tests, the algorithm was still not implemented in a micro-controller, and as a result this had to be tested off-line.

The vehicle used was FST06e Fig. 3, a rear wheel drive electric car with two independent motors. The vehicle itself is equipped with a steering encoder, a GPS and an IMU with a 3-axis accelerometer (ADXL345), a 3-axis gyroscope (L3G4200D) and a 3-axis magnetometer (HMC5883L). The actual torque applied to each driven wheel is retrieved from the motors. The vehicle was also equipped with a DGPS to provide a ground truth of the sideslip angle. The vehicle acquisition system, and the DGPS are completely independent systems with separate logging units, and both data are only crossed during the presented graphs. More detailed information of the acquisition system can be found in [9].

The ACF and PCF results are shown and discussed in [9] and for that reason a special focus will be given to the vehicle estimator in this work. Since the data was used off-line, it was possible to have

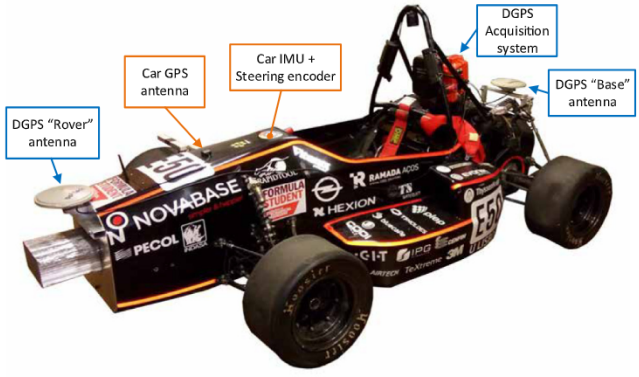

Fig. 3. FST06e equipped for the presented tests. Orange: location of the vehicle sensors. Blue: location of the DGPS parts.

Table 1
FST06e technical specifications.

Wheelbase	Track	Mass	Yaw inertia	Weight dist.	Cornering stiffness	
–	tr	m	I_ψ	–	$C_{\alpha f}$	$C_{\alpha r}$
1.59	1.24	356	120	45–55	15 270	19 950
m	m	kg	kg m^2	–	N/rad	N/rad

all sensor sources at the same frequency for the vehicle, that was defined as 100 Hz, which allowed the use of the algorithm at the same frequency. The DGPS was logged at 10 Hz, and the presented data is the raw values. The trajectory of the vehicle was limited to a 60 × 20 meters area. It started moving at instant $t = 164$ s, with some straight trajectories interspersed with curves. At $t = 223$ s made several turns at a constant speed and radius for one side, and at $t = 265$ s made the same to the other side.

First is presented the Vehicle Linear Estimator (VLE), which has the advantage of being linear, and as such, easier to implement and computationally lighter. The estimator used was already presented (13), and is based on the linear system of the planar movement of the vehicle (11). For this system, the technical specifications of the FST06e, that are condensed in Table 1, were used. The gains applied were identified using the discrete Kalman Filter theory, starting with the variance of the noise used, and then fine-tuned by hand for the application. Since the system chosen is time-varying, a set of gains was identified *a priori* for each longitudinal velocity, and then a lookup table was implemented.

The results obtained are presented in Fig. 4(a), where the data from the DGPS is depicted in blue, and in orange the result of the algorithm of Fig. 1 using the VLE. As can be seen, the VLE can accompany the fast dynamics of the system quite well with little error, apart from the constant speed and radius turns. In these

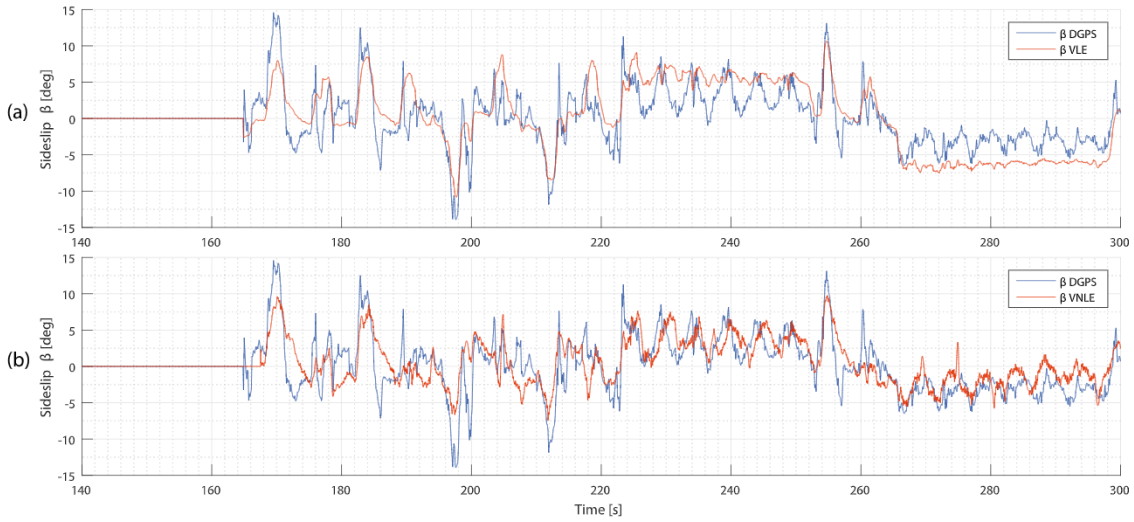

Fig. 4. Results of the estimators (a) VLE and (b) VNLE. Ground truth in blue. (For interpretation of the references to color in this figure legend, the reader is referred to the web version of this article.)

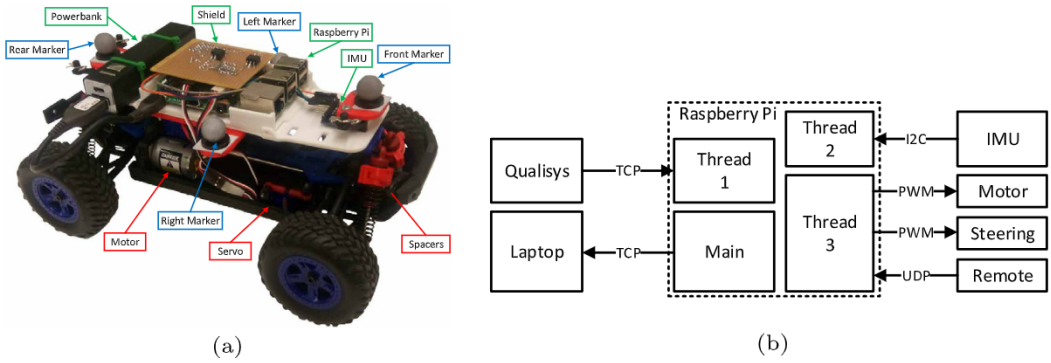

Fig. 5. RC vehicle used to test the algorithm. (a) hardware (b) software and protocols.

turns, the VLE misses by far the oscillations, resulting in an almost constant value. These oscillations are a result of a small banking in the track, that combined with some road paint results in several changes between slip and traction of the wheels.

For the VNLE, it was used the theory of the Discrete Extended Kalman Filter. In this case, since the system is time-varying with all the states, the gains had to be computed at each iteration. These were identified using the same method of the VLE, starting with the sensors variance, and then fine-tuned. The obtained results are depicted in Fig. 4(b), and is clear that this is a noisier output than the VLE. Until $t = 220$ s, the results of the VNLE are very similar to the VLE, but the most significant difference is in the constant speed and radius turns, where the estimate can follow the oscillations quite well. Between the estimate and the DGPS output there is a slight offset, easy to see around $t = 226$ s to $t = 250$ s. This is associated with the time synchronization of the two logging systems.

Comparing both estimators, it is clear that the VNLE has a better performance compared with the VLE in the constant speed and radius turns. However, using the Sprague and Geers metrics [16] in Table 2, it is clear that the overall performance (C) of the VLE is better than that of the VNLE. Therefore, the VLE proves to be an option when the test conditions are inside the linearization limits. In both figures, until the vehicle starts to move, the sideslip angle is perfectly zero, this is due to a rule implemented for $v_x < 3$ m/s there is no sideslip, to protect the results from numerical instability during low velocities.

Table 2
Sprague and Geers validation metric for the estimators.

Estimator	M	P	C
VLE	0.1805	0.2145	0.2804
VNLE	−0.2128	0.2485	0.3272

4. On-board implementation

To test the feasibility of running the algorithm in real-time in a Formula Student Prototype, an implementation was made in a RC car with a micro-controller. An RC car was used, as it provided a method for verifying the viability of the algorithm in an online application, allowed the use of an indoor multi-camera motion capture system with millimetric precision, and because the availability and access of the FST06e vehicle were limited due to it being an ongoing project. Additionally, it was intended to validate that the algorithm could be processed at 100 Hz in real time by a small micro-controller.

A 1:18 scale radio-controlled (RC) car, Fig. 5(a), with a single motor and four-wheel drive was modified. The micro-controller chosen is a Raspberry Pi 3 model B, due to the integrated wireless capabilities. As depicted in Fig. 5(b), the Raspberry Pi is the center of all computation with the created program divided in a main cycle and three threads. The first one is connected to a computer running the Qualisys® Track Manager software (QTM), that uses six infra-red cameras to triangulate the position of the four markers placed on the car, and then transmits it to the Raspberry Pi. The second thread communicates through I2C to the IMU. The third

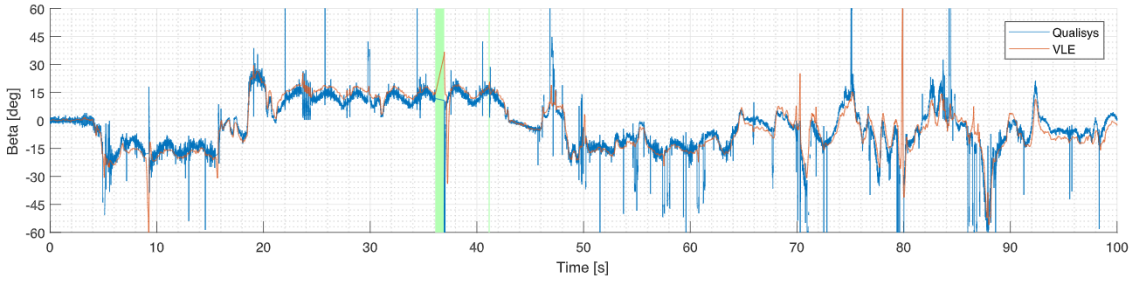

Fig. 6. Sideslip estimation of VLE (orange), ground truth (blue). (For interpretation of the references to color in this figure legend, the reader is referred to the web version of this article.)

thread receives through UDP (User Datagram Protocol) the inputs from a remote controller and converts it to PWM (Pulse Width Modulation) in order to control the motor and the steering servo motor. The main program receives the data from all the threads and runs the algorithm. The results are then sent by TCP (Transmission Control Protocol) to a computer for visualization. Since it was not viable to access the torque applied from this motor, it was not possible to test the VNLE.

Since QTM can provide in real-time both positions and angles, it is used as the ground truth for the implementation. During the tests a problem was detected with the environment. Since the laboratory is full of machinery and electric equipment, the magnetometer for the ACF could not provide a decent measurement. The solution was to introduce the yaw angle measurement from the QTM in parallel with the magnetometer reading.

For FST06e cornering stiffness values were known, but for this vehicle cornering stiffness values were unknown so they had to be identified. The test consisted in a trajectory performed at a constant velocity and with small steering angles as required by the model, that resulted in the transition and input matrices depicted in (17). These matrices were correlated with the base system (11) and resulted in the continuous system (18) to be used in the VLE. The gain identification for the filter had the same process as before, and a lookup table implemented with the gains dependent of the longitudinal velocity.

$$A_{identified} = \begin{bmatrix} -4.473 & -0.114 \\ -0.070 & -8.633 \end{bmatrix}, \quad B_{identified} = \begin{bmatrix} 1.174 \\ 22.87 \end{bmatrix} \tag{17}$$

$$\begin{bmatrix} \dot{v}_y \\ \dot{\psi} \end{bmatrix} = \begin{bmatrix} \dfrac{3.4576}{v_x} & \dfrac{0.5298}{v_x} - v_x \\ -0.07032 & -6.6733 \end{bmatrix} \begin{bmatrix} v_y \\ \psi \end{bmatrix} + \begin{bmatrix} 1.371 \\ 22.87 \end{bmatrix} \delta \tag{18}$$

The result of the estimation algorithm is depicted in Fig. 6 in orange. The ground truth (blue) is given by the raw numerical differentiation of the QTM position output. As can be seen, the estimate output of the sideslip angle has results very close to the validation signal, with only a slight offset for higher sideslip angles as expected from the linear estimator. Even so, the estimate could acquire all the dynamics of the system, even the fastest ones.

In Fig. 6 it is also possible to see two green zones ($t = 37$ s and $t = 41$ s). In these intervals there is a lack of data, as if the operating system had frozen. The problem was not identified, but is likely linked to an insufficient source of power due to background processes, as these flaws are not regular or periodic.

5. Conclusion

A self-calibrating algorithm for estimating the sideslip angle of a Formula Student vehicle was presented in two versions, a linear and a non-linear. This algorithm was tested with real data from a Formula Student prototype and implemented in a micro-controller. The test with real data had a differential GPS for ground truth validation. The results from the non-linear estimator proven to be considerably better than the linear. Nevertheless, the VLE also produced acceptable results with a C (Sprague and Geers) of 0.2804, especially for lower sideslip angles, when the working zone is closer to the linearization assumptions. The implementation in the micro-controller also fulfilled its objective of proving that the algorithm could work in a small hardware at a high frequency (100 Hz). The results of the estimate were also very satisfactory, with the output close to the ground truth, even with the linear estimator.

Acknowledgments

This work was supported by FCT, Portugal, through IDMEC, under LAETA, project UID/EMS/50022/2013. The authors also thank the prompt and fruitful cooperation with the IST Formula Student team, FST Lisboa.

References

[1] L.D. Novellis, A. Sorniotti, P. Gruber, A. Pennycott, Comparison of feedback control techniques for torque-vectoring control of fully electric vehicles, IEEE Trans. Veh. Technol. 63 (8) (2014) 3612–3623, http://dx.doi.org/10.1109/TVT.2014.2305475.
[2] C. Geng, L. Mostefai, M. Denai, Y. Hori, Direct yaw-moment control of an in-wheel-motored electric vehicle based on body slip angle Fuzzy observer, IEEE Trans. Ind. Electron. 56 (5) (2009) 1411–1419, http://dx.doi.org/10.1109/TIE.2009.2013737.
[3] T. Chung, K. Yi, Design and evaluation of side slip angle-based vehicle stability control scheme on a virtual test track, IEEE Trans. Control Syst. Technol. 14 (2) (2006) 224–234, http://dx.doi.org/10.1109/TCST.2005.863649.
[4] M. Doumiati, A.C. Victorino, A. Charara, D. Lechner, Onboard real-time estimation of vehicle lateral tire–road forces and sideslip angle, IEEE/ASME Trans. Mechatronics 16 (4) (2011) 601–614, http://dx.doi.org/10.1109/TMECH.2010.2048118.
[5] D.M. Bevly, J. Ryu, J.C. Gerdes, Integrating INS sensors with GPS measurements for continuous estimation of vehicle sideslip, roll, and tire cornering stiffness, IEEE Trans. Intell. Transp. Syst. 7 (4) (2006) 483–493, http://dx.doi.org/10.1109/TITS.2006.883110.
[6] H.F. Grip, L. Imsland, T.A. Johansen, J.C. Kalkkuhl, A. Suissa, Vehicle sideslip estimation, IEEE Control Syst. 29 (5) (2009) 36–52, http://dx.doi.org/10.1109/MCS.2009.934083.
[7] M. Abdulrahim, On the dynamics of automobile drifting, in: SAE Technical Paper, SAE International, 2006, http://dx.doi.org/10.4271/2006-01-1019.
[8] A. Antunes, C. Cardeira, P. Oliveira, Sideslip estimation of formula student prototype through GPS/ins fusion, in: 2017 IEEE International Conference on Autonomous Robot Systems and Competitions (ICARSC), 2017, pp. 184–191, http://dx.doi.org/10.1109/ICARSC.2017.7964073.
[9] A. Antunes, C. Cardeira, P. Oliveira, Application of sideslip estimation architecture to a formula student prototype, in: A. Ollero, A. Sanfeliu, L. Montano, N. Lau, C. Cardeira (Eds.), ROBOT 2017: Third Iberian Robotics Conference. ROBOT 2017. Advances in Intelligent Systems and Computing, Vol. 694, Springer, Cham, 2018, pp. 409–421, http://dx.doi.org/10.1007/978-3-319-70836-2_34.
[10] R.G. Brown, P. Hwang, Introduction to Random Signals and Applied Kalman Filtering: with MATLAB Exercises, fourth ed., Wiley, 2012, (ISBN:978-0470609699).
[11] J.F. Vasconcelos, G. Elkaim, C. Silvestre, P. Oliveira, B. Cardeira, Geometric approach to strapdown magnetometer Calibration in sensor frame, IEEE Trans. Aerosp. Electron. Syst. 47 (2) (2011) 1293–1306, http://dx.doi.org/10.1109/TAES.2011.5751259.
[12] R.N. Jazar, Vehicle Dynamics: Theory and Applications, first ed., Springer, 2008, (ISBN:978-0387742434).
[13] J. Ryu, E.J. Rossetter, J.C. Gerdes, Vehicle sideslip and roll parameter estimation using GPS, in: Proceedings of the AVEC International Symposium on Advanced Vehicle Control, 2002, pp. 373–380.

[14] K. Nam, S. Oh, H. Fujimoto, Y. Hori, Estimation of sideslip and roll angles of electric vehicles using lateral tire force sensors through RLS and kalman filter approaches, IEEE Trans. Ind. Electron. 60 (3) (2013) 988–1000, http://dx.doi.org/10.1109/TIE.2012.2188874.
[15] U. Kiencke, L. Nielsen, Automotive Control Systems for Engine, Driveline, and Vehicle, second ed., Springer, 2005, (ISBN:978-3540231394).
[16] T.L. Geers, An objective error measure for the comparison of calculated and measured transient response histories, Shock and Vibration Informa- tion Center The Shock and Vibration Bull. 54, Pt. 2 p 99-108(SEE N 85-18388 09-39).

André Antunes is a recently graduated student from Instituto Superior Técnico (IST), Lisbon, Portugal. He completed his master's degree in mechanical engineering with a thesis on Sideslip Estimation of Formula Student Prototype. He was a member of the formula student team.

He is currently working at Tekever.

His research interests include automobiles and estimation methods.

Pedro Outeiro is a recently graduated student from Instituto Superior Técnico (IST), Lisbon, Portugal. He completed his master's degree in mechanical engineering with a thesis on Control and Estimation Methods for Unknown Load Transportation with Quadrotors. He received three diplomas for academic excellence and one for academic merit during his studies.

He is aiming to further his studies by enrolling into a Phd programme, allowing him also to continue the work he started with his master's thesis.

Carlos B. Cardeira was born in Quinjenje, Angola, and received the engineering and master of science degrees in 1986 and 1991, in electrical engineering from Instituto Superior Técnico in Lisbon — Portugal. In 1994 he received the PhD in electrical engineering and computer science from the Institut National Polytechnique de Lorraine in Nancy — France. He is a member of the Center of Intelligent Systems of the IDMEC research laboratory and teaches at Instituto Superior Técnico in Lisbon courses in Mechatronics Systems, Industrial Automation and Informatics areas. He made several post-docs and sabbatical leaves, namely in IRIT and LAAS in Toulouse-France, CERN in Geneva — Switzerland and Schneider-Electric in Seligenstadt-Germany.

Paulo Oliveira (Hab 16 Ph.D.'02 M.Sc.'91) received the "Licenciatura," M.S., and Ph.D. degrees in Electrical and Computer Engineering, and the Habilitation in Mechanical Engineering from Instituto Superior Técnico (IST), Lisbon, Portugal, in 1991, 2002, and 2016, respectively. He is an Associate Professor in the Department of Mechanical Engineering of IST and Senior Researcher in the Associated Laboratory for Energy, Transports, and Aeronautics. His research interests are in the area of autonomous robotic vehicles with a focus on the fields of estimation, sensor fusion, navigation, positioning, and mechatronics. He is author or coauthor of more than 65 journal papers and 175 conference communications. He participated in more than 30 European and Portuguese research projects, over the last 30 years.